Role of Solid-State Miscibility during Anion Exchange in Cesium Lead Halide Nanocrystals Probed by Single-Particle Fluorescence

Dong Wang[1], John Cavin[2], Bo Yin[3], Arashdeep S. Thind[3], Albina Y. Borisevich[4], Rohan Mishra[5,3], Bryce Sadtler[1,3]*

[1]Department of Chemistry, Washington University, St. Louis, Missouri 63130

[2]Department of Physics, Washington University, St. Louis, Missouri 63130

[3]Institute of Materials Science & Engineering, Washington University, St. Louis, Missouri 63130

[4]Center for Nanophase Materials Sciences, Oak Ridge National Laboratory, Oak Ridge, Tennnessee, 37831

[5]Department of Mechanical Engineering and Materials Science, Washington University, St. Louis, Missouri 63130

* To whom correspondence should be addressed. Email: sadtler@wustl.edu

Abstract

In this Letter, we used fluorescence microscopy to image the reversible transformation of individual $CsPbCl_3$ nanocrystals to $CsPbBr_3$, which enables us to quantify heterogeneity in reactivity among hundreds of nanocrystals prepared within the same batch. We observed a wide distribution of waiting times for individual nanocrystals to react as has been seen previously for cation exchange and ion intercalation. However, a significant difference for this reaction is that the switching times for changes in fluorescence intensity are dependent on the concentration of substitutional halide ions in solution (i.e., Br^- or Cl^-). Based on the high solid-state miscibility between $CsPbCl_3$ and $CsPbBr_3$, we develop a model in which the activation energy for anion exchange depends on the density of exchanged ions in the nanocrystal. The heterogeneity in reaction kinetics observed among individual nanocrystals limits the compositional uniformity that can be achieved in luminescent $CsPbCl_{3-x}Br_x$ nanocrystals prepared by anion exchange.

TOC graphic

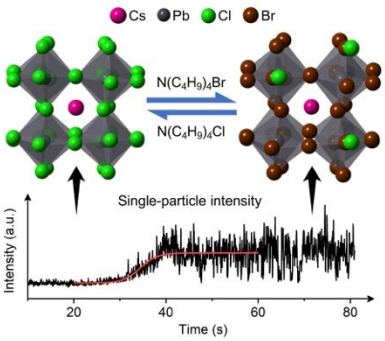

Colloidal cesium lead halide nanocrystals ($CsPbX_3$ where X = Cl, Br or I) display high photoluminescence (PL) quantum yields without the need for post-synthetic processing.[1-9] The wavelength of emission can be tuned across the visible range based on their size and composition making these materials of significant interest for applications in light emission, such as light-emitting diodes and lasers.[10-12] Anion exchange provides a facile method to tune the halide composition and bandgap of $CsPbX_3$ and $CH_3NH_3PbX_3$ nanocrystals (NCs).[6-7, 13-16] Similar to other solid-state transformations in nanocrystals (e.g., cation exchange and ion intercalation),[17-28] the high surface-to-volume ratio and diffusion coefficients of ions enable this reaction to take place both rapidly (i.e., on the time scale of seconds to minutes) and reversibly. For applications in solid-state lighting, it is desirable to synthesize lead halide perovskite nanocrystals of uniform size and composition as heterogeneity in these parameters lowers the color purity. However, the interconversion between $CsPbX_3$ nanocrystals of different halide compositions via anion exchange exhibits complex reaction kinetics. Both the lattice constants and PL emission wavelength have been observed to go through different rates of change as the reaction progresses.[29-30] These changes in reaction rate are supported by first-principles calculations that indicate $CsPbCl_{3-x}Br_x$ and $CsPbBr_{3-x}I_x$ mixed-halide crystals with x = 2 are more stable than other halide compositions and may act as an intermediate phase to hinder a continuous transformation.[30-32] Furthermore, the kinetics for the $CsPbBr_3/CsPbI_3$ exchange pair have been shown to be sensitive to the surface chemistry of the nanocrystals and the method used to monitor the reaction (e.g., diffraction or photoluminescence). These observations suggest that fundamental studies on the kinetics of anion exchange in individual $CsPbX_3$ nanocrystals are needed to facilitate their production and incorporation into optoelectronic devices.

While anion exchange exhibits similarities to other chemical transformations in colloidal semiconductor nanocrystals, a unique feature of this reaction is the complete solid-state miscibility exhibited between $CsPbCl_3$ and $CsPbBr_3$.[31-32] In this study, we aimed to determine how this high miscibility affects the reaction trajectories of individual nanocrystals undergoing anion exchange. Single-nanocrystal fluorescence microscopy been used to understand how heterogeneity among a population of particles leads to the observed ensemble behavior.[8-9, 21-23, 33-45] Thus, we used changes in the emission wavelength and intensity as a signature for when individual NCs undergo this transformation. We observed distinct differences for this system compared to related solid-state transformations where the initial and final crystals lack solid-solubility.[21-23] Based on our observations and previous ensemble kinetic studies, we develop a model in which the decrease in activation barrier for successive anion exchange events is more gradual than systems that require a phase transformation. Our results imply that the stochastic nature of reactivity among individual nanocrystals limits the compositional uniformity that is possible in $CsPbCl_{3-x}Br_x$ nanocrystals prepared by anion exchange.

Figure 1a shows a bright-field transmission electron microscopy (TEM) image of $CsPbCl_3$ NCs synthesized using the method of Kovalenko and coworkers.[1] The NCs are platelet shaped with an average edge length of 19.1 ± 5.0 nm (average ± 1st standard deviation). The $CsPbCl_3$ NCs were converted to cesium lead chlorobromide ($CsPbCl_{3-x}Br_x$) NCs on a TEM grid via anion exchange using tetrabutylammonium bromide (TBAB) as the source of bromide anions. As shown in Figure 1b, the shape and size of the $CsPbCl_{3-x}Br_x$ NCs, which have an average edge length of 19.4 ± 3.9 nm (average ± 1st standard deviation), was preserved after anion exchange. The Supporting Information provides detailed experimental procedures for synthesizing $CsPbCl_3$ NCs

and converting them to $CsPbBr_3$ as well as histograms showing the edge lengths before and after anion exchange (Figure S1).

Figure 1c shows powder x-ray diffraction (XRD) patterns of the $CsPbCl_3$ NCs before and after anion exchange. The XRD pattern of the $CsPbCl_3$ NCs matched the expected diffraction pattern for orthorhombic $CsPbCl_3$. Peaks in the XRD pattern of the converted $CsPbCl_{3-x}Br_x$ NCs showed a shift to smaller angles compared to the pattern for $CsPbCl_3$. However, the peaks for the product NCs were still at higher angles relative to the expected diffraction pattern for orthorhombic $CsPbBr_3$, which indicates that the product NCs contain residual chloride ions. The presence of chloride in the product NCs following anion exchange was further confirmed by x-ray photoelectron spectroscopy (XPS) (see Figure S3 and Table S2). Assuming a linear shift in lattice constant with anion composition, as reported for alloys using first-principles calculations,[31] the approximate composition after anion exchange is $CsPbClBr_2$ (i.e., x = 2). The presence of Cs_4PbBr_6 as an impurity is observed when the $CsPbCl_{3-x}Br_x$ NCs were prepared for XRD analysis in which a higher concentration of NCs was used than for TEM and fluorescence microscopy (Figure 1c and Figure S2).[24-27] As Cs_4PbBr_6 has been reported to be non-fluorescent at visible wavelengths,[24-27] this impurity phase does not show up in the fluorescence microscopy studies described below.

To further investigate the localized structural changes occurring within individual nanocrystals as a result of the anion exchange, we have performed atomic resolution scanning transmission electron microscope (STEM) imaging. Figure 1d and 1e show atomic resolution high-angle annular dark field (HAADF) images of single $CsPbCl_3$ and $CsPbCl_{3-x}Br_x$ nanocrystals, respectively, viewed along the [101] direction of the orthorhombic polymorph. In this imaging mode, the intensity of individual atomic columns is approximately proportional to the squared

atomic number (~Z^2) of the column.[46] Hence, the brightest atomic columns correspond to Pb-(Cl/Br) followed by the Cs atomic columns. The lighter Cl (Z = 17) atomic columns in $CsPbCl_3$ (Figure 1d) are not visible as they cause weak elastic scattering of the electrons. However, the mixed Cl/Br columns in $CsPbCl_{3-x}Br_x$ (Figure 1e) are visible because of the heavier Br atoms (Z = 35). We do not observe any discernible segregation of Cl/Br ions, which would have resulted in missing anion columns that were rich in Cl. As shown in Figure 1c, the anion exchange process is accompanied by the shifts in the XRD pattern to lower angles because of the increase in lattice constant of the ensemble as the concentration of Br increases. Based on STEM-HAADF image analysis, we provide the changes in Cs-Cs (Δ) and Pb-Cs (δ) in-plane bond distances within individual $CsPbCl_3$, $CsPbCl_{3-x}Br_x$ and $CsPbBr_3$ nanocrystals in Figure 1f and compare them with previously reported bond distances.[47] The average Δ (Cs-Cs) from HAADF images for $CsPbCl_3$ and $CsPbBr_3$ nanocrystals is 5.58 ± 0.04 and 5.85 ± 0.04 Å, respectively, which compares well with the reported values of 5.59 and 5.84 Å. Similarly, δ (Pb-Cs) from HAADF images for $CsPbCl_3$ and $CsPbBr_3$ nanocrystals is 3.95 ± 0.05 and 4.14 ± 0.05 Å respectively. They are in good agreement with the reported values of 3.96 and 4.14 Å for $CsPbCl_3$ and $CsPbBr_3$, respectively. Both Δ (Cs-Cs) and δ (Pb-Cs) increase as the concentration of Br increases, and the values of Δ = 5.65 ± 0.04 Å and δ = 4.00 ± 0.04 Å for $CsPbCl_{3-x}Br_x$ are intermediate between the two end members. Using Vegard's law, both measurements lead to an average composition with x = 0.76 ± 0.04. Thus, STEM-HAADF imaging reveals a steady lattice expansion of individual NCs upon Cl/Br exchange with no apparent clustering of the halide ions.

Optical spectroscopy was next used to monitor anion exchange in $CsPbX_3$ NCs based on systematic shifts in the optical band gap with composition.[1, 4, 6, 13] Figure 2a shows UV-vis absorption and PL spectra of colloidal solutions of both $CsPbCl_3$ and $CsPbCl_{3-x}Br_x$ NCs. The

maxima in the first exciton absorption peak shifted from 390 nm for the initial $CsPbCl_3$ NCs to 492 nm after anion exchange, similar to previous reports.[1-2, 6, 13] Furthermore, the integrated PL intensity increased by over 30 times after anion exchange, consistent with the higher PL quantum yield typically exhibited by $CsPbBr_3$ compared to $CsPbCl_3$ NCs.[7] Both the initial and product NCs exhibit weak quantum confinement based on the appearance of exciton peaks and the blue shift of the fluorescence maxima relative to the bulk band gaps of $CsPbCl_3$ and $CsPbBr_3$.[1] Although the average edge length of the platelet nanocrystals is over 19 nm, the thicknesses of the nanoplates vary from 3 to 5 nm (see Figure S4), which leads to quantum confinement, similar to previous reports.[3, 6, 36, 48] Figure 2b shows the change in PL spectra after successive aliquots of TBAB were added to a colloidal solution of $CsPbCl_3$ nanocrystals. The maxima in the PL spectra red shifted continuously from 398 nm (3.12 eV) to 505 nm (2.46 eV) as the total amount of TBAB added was increased (Figure 2c). The full widths at half maxima for the PL spectra varied between 0.09 and 0.13 eV (see Table S1). This gradual shifting is a result of the high miscibility of $CsPbCl_3$ and $CsPbBr_3$ along with rapid exchange kinetics for nanoscale crystals such that the anion composition in the nanocrystal lattice reflects the overall ratio of Cl^- to Br^- anions.[13, 15, 29]

We used the red shift and increase in PL intensity upon anion exchange from Cl^- to Br^- to monitor this transformation in single NCs by fluorescence microscopy. The experimental setup is similar to that used in our previous studies on ion intercalation in $PbBr_2$ nanocrystals[23] as well as work by Routzahn and Jain on cation exchange in CdSe nanocrystals.[21-22] The SI provides further details of the procedure and a schematic of the experimental setup (Figure S6). Briefly, the stock solution of $CsPbCl_3$ NCs is diluted (250×) and spin-coated onto a microscope coverslip which forms the bottom half of a flow cell. A TBAB solution of varying concentration (1 to 10 μg/mL) dissolved in 1-octadecene (ODE) and tert-butanol (25:1 volume ratio) is then introduced into the

flow cell using a syringe pump. Ultraviolet illumination (315 – 380 nm) is sent through the objective of an inverted microscope to photoexcite NCs on the coverslip. However, an emission filter cuts off emission from the $CsPbCl_3$ NCs, and so the initial field-of-view is dark. While there is heterogeneity in the fluorescence maximum for different nanocrystals, our ability to watch individual nanocrystals undergo anion exchange relies on the large spectral shift (~100 nm) and increased fluorescence brightness during this reaction. After the TBAB solution is introduced, fluorescent spots begin to appear in the field-of-view, indicating the transformation of $CsPbCl_3$ NCs to $CsPbCl_{3-x}Br_x$ (see Supporting Movie).

Figure 3a-d shows a section of the microscope field-of-view at different times during the transformation of individual NCs at a TBAB concentration of 1 μg/mL (3.1 μmol/L); a typical field-of-view contained ~500 NCs. Changes in fluorescence intensity integrated over of the entire field-of-view following the introduction of TBAB are shown in Figure 3e, f for two different TBAB concentrations (1 and 10 μg/mL). The integrated intensity rise is more abrupt at the higher TBAB concentration. For TBAB concentrations lower than 1 μg/mL, the appearance of bright fluorescent spots was not observed. At TBAB concentrations greater than 10 μg/mL (31 μmol/L), emission from individual NCs was observed to degrade at a similar timescale to the transformation. We used a light intensity (15 $\mu W/cm^2$ at 350 nm) that is lower than the intensities (mW/cm^2 to W/cm^2) typically needed to observe photoinduced reactions in lead halide perovskite films, such as halide segregation.[9, 49-52] Furthermore, we observed the same trends in single-particle reaction trajectories when using different excitation wavelengths and intensities (see the Supporting Discussion and Figure S15).

Representative intensity trajectories for individual NCs at different TBAB concentrations are shown in Figure 3e, f. Once the exchange reaction has occurred, emission from individual $CsPbCl_{3-}$

$_xBr_x$ NCs exhibited fluorescence intermittency as has been previously observed for lead halide perovskite nanocrystals.[38-42] Blinking in $CsPbCl_{3-x}Br_x$ NCs prepared by in situ anion exchange under the microscope was similar to NCs that were converted prior to imaging (Figure S8). TEM images at different dilution factors (see Figure S7) indicate that the particle concentration used for fluorescence microscopy led to well dispersed nanocrystals with few clusters. Furthermore, clusters of nanocrystals with overlapping emission profiles within a diffraction-limited region could be distinguished from single nanocrystals based on their intensity profiles (Figures S9 and S10)[44-45] and were removed from subsequent analysis. A wide range of turn-on times was observed for different NCs within the same field-of-view, similar to other solid-state transformations that have been studied by fluorescence microscopy.[21-23]. At the flowrate used in these experiments (7.5 mL/hour), the turn-on times for individual NCs were not correlated with their location (Figure S11). Thus, the slow rise in the integrated intensity for the ensemble of NCs is attributed to the stochastic nature of turn-on events for individual NCs.

To quantify differences in the fluorescence trajectories of individual NCs, the time needed for each NC to reach a threshold intensity (three standard deviations above the noise) was measured for hundreds of NCs at different concentrations of TBAB. We refer to this value as the waiting time for the NC to turn on. To compare the distribution of waiting times at different concentrations of TBAB, the first NC to turn on at a given TBAB concentration was assigned a waiting time of 0, and the waiting times for all other NCs in the field-of-view were measured relative to the first one. Histograms of the relative waiting times for single NCs transformed using different concentrations of TBAB are plotted in Figure S12. These distributions were fit to Gaussian functions as shown in Figure 4a. The distributions of waiting times show a strong dependence on

the TBAB concentration. As the TBAB concentration increases, both the mean relative waiting time and the full width at half maximum (FWHM) of the Gaussian fit decrease (Figure S13).

The waiting time for each NC to turn on includes an "incubation time" in which the TBAB solution has entered the field-of-view, but the NC has not yet started to transform. To exclude the incubation component, we next fit the intensity rise for each NC trajectory to a sigmoidal function to extract the switching time, τ, for the NC.[21-23] A sharper intensity rise will lead to a smaller switching time. As shown in Figure 4b, both the mean value of single-NC switching times and the standard deviation in the distribution of switching times decrease as the TBAB concentration increases. Thus, the sharper integrated intensity rise for the ensemble of NCs at higher TBAB concentration (see Figure S14) results from both the narrowing of the distribution of waiting and switching times and their shift towards shorter times. While a systematic investigation of how the waiting and switching times depend on the shape and size of the NCs is ongoing, these same trends were observed for anion exchange in $CsPbCl_3$ NCs with larger average dimensions (Figure S16). We also investigated the back conversion of $CsPbCl_{3-x}Br_x$ NCs to $CsPbCl_3$ with tetrabutylammonium chloride (TBAC) as the chloride source. Using the same analysis as described above for the forward transformation, the $CsPbCl_{3-x}Br_x$ NCs are initially bright under the microscope and become dark after they transform to $CsPbCl_3$ (Figure S17 and Supporting Movie). Both the mean values of waiting times and switching times for the back exchange of single NCs show a similar dependence on the TBAB concentration as the forward transformation (Figure S18).

Single-particle fluorescence microscopy has been previously used to study cation exchange between CdSe and Ag_2Se NCs as well as the intercalation of CH_3NH_3Br into $PbBr_2$ NCs to form $CH_3NH_3PbBr_3$.[21-23] Waiting and switching times for these transformations were measured as a function of reactant concentration (i.e., $AgNO_3$ or CH_3NH_3Br). Similar to our results, in both cases

the distribution of waiting times narrowed as the reactant concentration increased. For all three reactions, the ensemble intensity rise comprises abrupt transitions for individual NCs that exhibit a distribution of incubation times before they transform. However, a significant difference observed in these prior cases was that the switching times were insensitive to the reactant concentration. We propose that differences in the solid-state miscibility between the initial and final crystals are responsible for the differences in switching times observed for these NC transformations. Both the CdSe/Ag_2Se and $PbBr_2$/$CH_3NH_3PbBr_3$ crystal pairs lack solid solubility due to differences in the arrangement of ions before and after the reaction.[17-18] Thus, in both of these transformations the new phase must first nucleate within the parent lattice. We previously simulated the effect of this phase transformation on waiting and switching times by incorporating an activation barrier for reaction events (e.g., ion intercalation or exchange) in a particle that decreased after a threshold number of events had been reached.[23] Monte Carlo trajectories were used to simulate the transformation of individual nanocrystals, and the probability for each reaction event depended on the free energy change for that step. When we incorporated a free energy change, ΔG_i (where i is the number of reaction events in a trajectory), that decreased after a critical number of reaction events, the simulated waiting times decreased with reactant concentration while the switching times were insensitive to concentration, matching experimental observations for solid-state transformations that lack solid solubility.

In the case of anion exchange between $CsPbCl_3$ and $CsPbBr_3$, the initial and final crystals possess complete solid miscibility due to their similarity in structure (both are orthorhombic) and anionic radii.[13, 32] Furthermore, activation barriers for halide diffusion in lead halide perovskites[15, 53] are smaller than for both Cd^{2+}/Ag^+ exchange in CdSe[54] as well as for $CH_3NH_3^+$ diffusion in lead halide crystals.[15, 53, 55] The high diffusion coefficients of halide anions within $CsPbX_3$ crystals lead

to a uniform composition within the nanocrystal as ions are exchanging in and out,[15-16, 29] which is confirmed by our atomic-resolution STEM characterization (Figure 1d-f). Based on these differences, we reasoned that the activation barrier for exchange events should decrease more gradually during anion exchange compared to the sudden change used in previous models for cation exchange in CdSe and ion intercalation in $PbBr_2$ NCs.[21-23] To test this hypothesis, we used Monte Carlo simulations that yield individual and ensemble nanocrystal transformation trajectories. We obtained the best match with the experimental results with a model where the energy required for exchanging an anion decreases quadratically with successive events (Figure S19). We refer to this as the exchange-density model because the number of exchanged ions neighboring a site is proportional to the local density of exchanges. The details of these simulations and descriptions of other models tested are provided in the SI. The quadratic function used in the exchange-density model leads to a more gradual increase in the probability for successive events compared to previous models for NC transformations that lack solid miscibility (Figure S20).

The results for the exchange-density model are shown in Figures 4c and S21. The simulated switching times of individual NC trajectories are significantly shorter than the overall switching time corresponding to the ensemble of nanocrystals, in agreement with the experimental data (Figure S21). Furthermore, both the median waiting times and median switching times depend on concentration with the switching times being smaller than the waiting times (Figure 4c). If successive exchange events instead have equal probability, then the waiting and switching times decrease at similar rates with increasing concentration, and simulated switching times for individual particles occur on the same timescale as the ensemble. On the other hand, models with a steeper drop in activation barrier for exchange events, such as the positive-cooperativity model developed by Routzahn and Jain,[21-22] lead to a switching time that is independent of concentration

(Figure S19). Thus, by assuming the halide concentration is uniform within each nanocrystal during the reaction, in agreement with our STEM results and prior ensemble kinetic studies,[29-30] our exchange-density model correctly describes both the stochasticity of anion exchange at the single-nanocrystal level and the concentration dependence of switching times.

In summary, analyzing the trajectories for single $CsPbCl_3$ NCs to transform into $CsPbBr_3$ (and vice versa) reveals a strong dependence for the switching times on the concentration of substitutional halide ions used to induce anion exchange. This concentration dependence has not been observed for other nanocrystal transformations, which we attribute to the lack of miscibility between the initial and final structures in these prior systems. We propose a model where the energetics for further anion exchange depend on the density of exchanged ions in the nanocrystal; this exchange-density model successfully reproduces all salient features of the reaction observed by single-particle fluorescence. Scaling up the synthesis of $CsPbCl_{3-x}Br_x$ nanocrystals will require homogeneous mixing of both the parent nanocrystals and substitutional halide ions at high concentrations to minimize the effect that the stochastic distribution of waiting times will have on the final halide composition (i.e., value of x) of individual nanocrystals. If reactant-depletion effects are prominent at higher concentrations, nanocrystals with longer waiting times may not undergo the same extent of anion exchange as those with shorter waiting times, leading to greater heterogeneity in composition and lower color purity. One way to achieve high-throughput synthesis with uniform mixing is through parallel microfluidic reactors as has been demonstrated for the synthesis of cadmium chalcogenide nanocrystals.[56]

Figure captions

Figure 1. (a) Bright-field TEM image of the as-synthesized $CsPbCl_3$ nanocrystals. (b) Bright-field

TEM image of $CsPbCl_{3-x}Br_x$ nanocrystals after anion exchange. (c) XRD patterns of the as-synthesized $CsPbCl_3$ nanocrystals (red) and the $CsPbCl_{3-x}Br_x$ (green) nanocrystals after anion exchange. The blue and gray traces show simulated powder XRD patterns made using ICSD collection code # 243735 for $CsPbBr_3$ and # 243734 for $CsPbCl_3$. The peaks marked with asterisks correspond to Cs_4PbBr_6. Atomic resolution STEM-HAADF images of (d) $CsPbCl_3$ and (e) $CsPbCl_{3-x}Br_x$ nanocrystals with their overlaid atomic model showing the [101] projection of the crystal structure. Scale bars correspond to 1 nm. (f) Comparison of the change in bond distances for different anion compositions as obtained from STEM-HAADF and those provided in a previous report.[47] Error bars correspond to one standard deviation in the spacing measurements.

Figure 2. (a) UV-visible absorption (solid lines) and PL (dashed lines) spectra of $CsPbCl_3$ nanocrystals dispersed in hexane before and after anion exchange. The spectra of the initial $CsPbCl_3$ nanocrystals are shown in grey, and the spectra of the $CsPbCl_{3-x}Br_x$ nanocrystals are shown in red. (b) Normalized PL spectra of $CsPbCl_3$ nanocrystals after the addition of increasing amounts of a TBAB solution in tert-butanol with a concentration of 10 mg/mL. 60 μL of the stock solution of $CsPbCl_3$ NCs was diluted by a factor of 50× for the ensemble anion exchange experiments. (c) Energies of the PL maxima for the same $CsPbCl_{3-x}Br_x$ nanocrystals as a function of the amount of TBAB added. The excitation wavelength was 300 nm for all PL spectra. Values of the peak positions and their corresponding FWHM are provided in Table S1.

Figure 3. (a-d) Selected frames from a fluorescence video recording during the transformation $CsPbCl_3$ nanocrystals to $CsPbCl_{3-x}Br_x$ at a TBAB concentration of 1 μg/mL (3.1 μmol/L). The scale bar of 10 μm applies to all four images, the contrast of the images has been inverted, and

only a portion of the entire microscope field-of-view is shown. (e) The integrated intensity versus time over the entire field-of-view (top) using a TBAB concentration of 1 μg/mL along with representative trajectories for individual nanocrystals (bottom). (f) The integrated intensity and single-particle intensities using a TBAB concentration of 10 μg/mL (31.1 μmol/L). The time points shown in the upper right corner of (a-d) as well as the x-axes of (e) and (f) were measured relative to when the TBAB solution was injected into the flow cell.

Figure 4. (a) Gaussian fits to distributions of relative waiting times for single NCs following anion exchange using different concentrations of TBAB. The original histograms are shown in Figure S12. (b) Experimental mean relative waiting times (black squares) and switching times (red triangles) for anion exchange in single NCs as a function of TBAB concentration. The error bars represent one standard deviation in the distribution of switching times. The lines show fits to the concentration dependencies of the form $y = [a/(x+b)] + c$ where a = 3 s·μg/mL, b = –0.7 μg/mL, and c = 1.5 s for the waiting times, and a = 6 s·μg/mL, b = 0.3 μg/mL, and c = 0.4 s for the switching times. (c) Simulated median waiting times (black squares) and switching times (red triangles) using the exchange-density model as a function of concentration. The solid lines show fits to the concentration dependences of the form $[a/x] + c$ where a = 40 and c = 0.15 for the waiting times, and a = 9.8 and c = 0.12 for the switching times in arbitrary units.

Associated content.

Acknowledgements.

This material is based upon work supported by the National Science Foundation under CHE-1753344 to B. S. JC was supported through NSF DMREF-1729787. A.S.T. and R.M. were

supported through NSF DMR-1806147. Aberration-corrected STEM experiments were conducted at the Center for Nanophase Materials Sciences at Oak Ridge National Laboratory, which is a Department of Energy (DOE) Office of Science User Facility, through a user project (AYB). Electron microscopy and x-ray photoelectron spectroscopy were performed at the Institute of Materials Science & Engineering at Washington University. X-ray diffraction was performed in the Department of Earth and Planetary Sciences at Washington University.

Supporting Information Available: Supporting Movies showing fluorescence videos where individual nanocrystals become bright as they transform from $CsPbCl_3$ to $CsPbCl_{3-x}Br_x$ and where individual nanocrystals become dark as they transform from $CsPbCl_{3-x}Br_x$ to $CsPbCl_3$, Materials and Methods, Supporting Discussion on the method used to identify single nanocrystals in fluorescence videos, the effect of flow rate and diffusion, the effect of the light intensity and wavelength on the single-nanocrystal trajectories, and a comparison of the different Monte Carlo models, Supporting Figures showing histograms of the edge lengths of the nanocrystals, a comparison of simulated XRD patterns for $CsPbBr_3$ and Cs_4PbBr_6, x-ray photoelectron spectra of the nanocrystal samples, STEM images of nanocrystals on their sides, a comparison of photoluminescence spectra of $CsPbBr_3$ nanocrystals synthesized by hot injection and anion exchange, a schematic of the experimental setup used to monitor anion exchange by fluorescence microscopy, TEM images of $CsPbCl_3$ nanocrystals deposited at different concentrations, a comparison of intensity trajectories for single nanocrystals prepared in situ and ex situ, intensity trajectories for clusters of particles, waiting times and switching times plotted vs. the position of the nanocrystals, plots of the distribution of waiting times at different TBAB concentrations, a comparison of the ensemble intensity rise and the mean switching time at different TBAB

concentrations, waiting times and switching times measured using different light intensities and wavelengths, waiting times and switching times for larger $CsPbCl_3$ nanocrystals, fluorescence trajectories for bromide to chloride anion exchange, a comparison of waiting and switching times for forward and backward exchange, simulated waiting and switching times for different models, changes in free energy and probability for exchange using different models, simulated reaction trajectories using the exchange-density model, and Supporting Tables listing the peak maxima and FWHM of ensemble PL spectra, binding energies measured by XPS, fitting parameters for different Monte Carlo models, and the ratios of fitting parameters. This material is available free of charge via the internet at http://pubs.acs.org

Author information.

*email: sadtler@wustl.edu

Conflicts of interest. The authors declare no competing financial interest.

References

(1) Protesescu, L.; Yakunin, S.; Bodnarchuk, M. I.; Krieg, F.; Caputo, R.; Hendon, C. H.; Yang, R. X.; Walsh, A.; Kovalenko, M. V., Nanocrystals of Cesium Lead Halide Perovskites ($CsPbX_3$, X = Cl, Br, and I): Novel Optoelectronic Materials Showing Bright Emission with Wide Color Gamut. *Nano Letters* **2015,** *15*, 3692-3696.

(2) Butkus, J.; Vashishtha, P.; Chen, K.; Gallaher, J. K.; Prasad, S. K. K.; Metin, D. Z.; Laufersky, G.; Gaston, N.; Halpert, J. E.; Hodgkiss, J. M., The Evolution of Quantum Confinement in $CsPbBr_3$ Perovskite Nanocrystals. *Chemistry of Materials* **2017,** *29*, 3644-3652.

(3) Cho, J.; Jin, H.; Sellers, D. G.; Watson, D. F.; Son, D. H.; Banerjee, S., Influence of Ligand Shell Ordering on Dimensional Confinement of Cesium Lead Bromide ($CsPbBr_3$) Perovskite Nanoplatelets. *Journal of Materials Chemistry C* **2017,** *5*, 8810-8818.

(4) Sapori, D.; Kepenekian, M.; Pedesseau, L.; Katan, C.; Even, J., Quantum Confinement and Dielectric Profiles of Colloidal Nanoplatelets of Halide Inorganic and Hybrid Organic–Inorganic Perovskites. *Nanoscale* **2016,** *8*, 6369-6378.

(5) Morrell, M. V.; He, X.; Luo, G.; Thind, A. S.; White, T. A.; Hachtel, J. A.; Borisevich, A. Y.; Idrobo, J.-C.; Mishra, R.; Xing, Y., Significantly Enhanced Emission Stability of $CsPbBr_3$ Nanocrystals Via Chemically Induced Fusion Growth for Optoelectronic Devices. *ACS Applied Nano Materials* **2018,** *1*, 6091-6098.

(6) Bekenstein, Y.; Koscher, B. A.; Eaton, S. W.; Yang, P.; Alivisatos, A. P., Highly Luminescent Colloidal Nanoplates of Perovskite Cesium Lead Halide and Their Oriented Assemblies. *Journal of the American Chemical Society* **2015,** *137*, 16008-16011.

(7) Di Stasio, F.; Christodoulou, S.; Huo, N.; Konstantatos, G., Near-Unity Photoluminescence Quantum Yield in $CsPbBr_3$ Nanocrystal Solid-State Films Via Postsynthesis Treatment with Lead Bromide. *Chemistry of Materials* **2017,** *29*, 7663-7667.

(8) Zhu, F.; Men, L.; Guo, Y.; Zhu, Q.; Bhattacharjee, U.; Goodwin, P. M.; Petrich, J. W.; Smith, E. A.; Vela, J., Shape Evolution and Single Particle Luminescence of Organometal Halide Perovskite Nanocrystals. *ACS Nano* **2015,** *9*, 2948-2959.

(9) Boote, B. W.; Andaraarachchi, H. P.; Rosales, B. A.; Blome-Fernández, R.; Zhu, F.; Reichert, M. D.; Santra, K.; Li, J.; Petrich, J. W.; Vela, J.*, et al.*, Unveiling the Photo- and Thermal-Stability of Cesium Lead Halide Perovskite Nanocrystals. *ChemPhysChem* **2019,** *20*, 2647-2656.

(10) Zhang, L.; Yang, X.; Jiang, Q.; Wang, P.; Yin, Z.; Zhang, X.; Tan, H.; Yang, Y.; Wei, M.; Sutherland, B. R.*, et al.*, Ultra-Bright and Highly Efficient Inorganic Based Perovskite Light-Emitting Diodes. *Nature Communications* **2017,** *8*, 15640-1-8.

(11) Van Le, Q.; Jang, H. W.; Kim, S. Y., Recent Advances toward High-Efficiency Halide Perovskite Light-Emitting Diodes: Review and Perspective. *Small Methods* **2018,** *2*, 1700419-1-18.

(12) Wang, K.; Wang, S.; Xiao, S.; Song, Q., Recent Advances in Perovskite Micro- and Nanolasers. *Advanced Optical Materials* **2018,** *6*, 1800278-1-27.

(13) Nedelcu, G.; Protesescu, L.; Yakunin, S.; Bodnarchuk, M. I.; Grotevent, M. J.; Kovalenko, M. V., Fast Anion-Exchange in Highly Luminescent Nanocrystals of Cesium Lead Halide Perovskites ($CsPbX_3$, X = Cl, Br, I). *Nano Letters* **2015,** *15*, 5635-5640.

(14) Jang, D. M.; Park, K.; Kim, D. H.; Park, J.; Shojaei, F.; Kang, H. S.; Ahn, J.-P.; Lee, J. W.; Song, J. K., Reversible Halide Exchange Reaction of Organometal Trihalide Perovskite Colloidal Nanocrystals for Full-Range Band Gap Tuning. *Nano Letters* **2015,** *15*, 5191-5199.

(15) Lai, M.; Obliger, A.; Lu, D.; Kley, C. S.; Bischak, C. G.; Kong, Q.; Lei, T.; Dou, L.; Ginsberg, N. S.; Limmer, D. T.*, et al.*, Intrinsic Anion Diffusivity in Lead Halide Perovskites Is Facilitated by a Soft Lattice. *Proceedings of the National Academy of Sciences* **2018,** *115*, 11929-11934.

(16) Pan, D.; Fu, Y.; Chen, J.; Czech, K. J.; Wright, J. C.; Jin, S., Visualization and Studies of Ion-Diffusion Kinetics in Cesium Lead Bromide Perovskite Nanowires. *Nano Letters* **2018,** *18*, 1807-1813.

(17) Son, D. H.; Hughes, S. M.; Yin, Y.; Paul Alivisatos, A., Cation Exchange Reactions in Ionic Nanocrystals. *Science* **2004,** *306*, 1009-1012.

(18) Hassan, Y.; Song, Y.; Pensack, R. D.; Abdelrahman, A. I.; Kobayashi, Y.; Winnik, M. A.; Scholes, G. D., Structure-Tuned Lead Halide Perovskite Nanocrystals. *Advanced Materials* **2016,** *28*, 566-573.

(19) Chan, E. M.; Marcus, M. A.; Fakra, S.; ElNaggar, M.; Mathies, R. A.; Alivisatos, A. P., Millisecond Kinetics of Nanocrystal Cation Exchange Using Microfluidic X-Ray Absorption Spectroscopy. *The Journal of Physical Chemistry A* **2007,** *111*, 12210-12215.

(20) Sadtler, B.; Demchenko, D. O.; Zheng, H.; Hughes, S. M.; Merkle, M. G.; Dahmen, U.; Wang, L.-W.; Alivisatos, A. P., Selective Facet Reactivity During Cation Exchange in Cadmium Sulfide Nanorods. *Journal of the American Chemical Society* **2009,** *131*, 5285-5293.

(21) Routzahn, A. L.; Jain, P. K., Luminescence Blinking of a Reacting Quantum Dot. *Nano Letters* **2015,** *15*, 2504-2509.

(22) Routzahn, A. L.; Jain, P. K., Single-Nanocrystal Reaction Trajectories Reveal Sharp Cooperative Transitions. *Nano Letters* **2014,** *14*, 987-992.

(23) Yin, B.; Cavin, J.; Wang, D.; Khan, D.; Shen, M.; Laing, C.; Mishra, R.; Sadtler, B., Fluorescence Microscopy of Single Lead Bromide Nanocrystals Reveals Sharp Transitions During Their Transformation to Methylammonium Lead Bromide. *Journal of Materials Chemistry C* **2019,** *7*, 3486-3495.

(24) Liu, Z.; Bekenstein, Y.; Ye, X.; Nguyen, S. C.; Swabeck, J.; Zhang, D.; Lee, S.-T.; Yang, P.; Ma, W.; Alivisatos, A. P., Ligand Mediated Transformation of Cesium Lead Bromide Perovskite Nanocrystals to Lead Depleted Cs_4PbBr_6 Nanocrystals. *Journal of the American Chemical Society* **2017,** *139*, 5309-5312.

(25) Wu, L.; Hu, H.; Xu, Y.; Jiang, S.; Chen, M.; Zhong, Q.; Yang, D.; Liu, Q.; Zhao, Y.; Sun, B.*, et al.*, From Nonluminescent Cs_4PbX_6 (X = Cl, Br, I) Nanocrystals to Highly Luminescent $CsPbX_3$ Nanocrystals: Water-Triggered Transformation through a CsX-Stripping Mechanism. *Nano Letters* **2017,** *17*, 5799-5804.

(26) Akkerman, Q. A.; Park, S.; Radicchi, E.; Nunzi, F.; Mosconi, E.; De Angelis, F.; Brescia, R.; Rastogi, P.; Prato, M.; Manna, L., Nearly Monodisperse Insulator Cs_4PbX_6 (X = Cl, Br, I) Nanocrystals, Their Mixed Halide Compositions, and Their Transformation into $CsPbX_3$ Nanocrystals. *Nano Letters* **2017,** *17*, 1924-1930.

(27) Li, M.; Zhang, X.; Dong, T.; Wang, P.; Matras-Postolek, K.; Yang, P., Evolution of Morphology, Phase Composition, and Photoluminescence of Cesium Lead Bromine

Nanocrystals with Temperature and Precursors. *The Journal of Physical Chemistry C* **2018,** *122*, 28968-28976.

(28) Li, M.; Zhang, X.; Matras-Postolek, K.; Chen, H.-S.; Yang, P., An Anion-Driven Sn^{2+} Exchange Reaction in $CsPbBr_3$ Nanocrystals Towards Tunable and High Photoluminescence. *Journal of Materials Chemistry C* **2018,** *6*, 5506-5513.

(29) Koscher, B. A.; Bronstein, N. D.; Olshansky, J. H.; Bekenstein, Y.; Alivisatos, A. P., Surface- Vs Diffusion-Limited Mechanisms of Anion Exchange in $CsPbBr_3$ Nanocrystal Cubes Revealed through Kinetic Studies. *Journal of the American Chemical Society* **2016,** *138*, 12065-12068.

(30) Loiudice, A.; Strach, M.; Saris, S.; Chernyshov, D.; Buonsanti, R., Universal Oxide Shell Growth Enables in Situ Structural Studies of Perovskite Nanocrystals During the Anion Exchange Reaction. *Journal of the American Chemical Society* **2019,** *141*, 8254-8263.

(31) Yin, W.-J.; Yan, Y.; Wei, S.-H., Anomalous Alloy Properties in Mixed Halide Perovskites. *The Journal of Physical Chemistry Letters* **2014,** *5*, 3625-3631.

(32) Bechtel, J. S.; Van der Ven, A., First-Principles Thermodynamics Study of Phase Stability in Inorganic Halide Perovskite Solid Solutions. *Physical Review Materials* **2018,** *2*, 045401-1-7.

(33) Empedocles, S.; Bawendi, M., Spectroscopy of Single CdSe Nanocrystallites. *Accounts of Chemical Research* **1999,** *32*, 389-396.

(34) Orfield, N. J.; McBride, J. R.; Keene, J. D.; Davis, L. M.; Rosenthal, S. J., Correlation of Atomic Structure and Photoluminescence of the Same Quantum Dot: Pinpointing Surface and Internal Defects That Inhibit Photoluminescence. *ACS Nano* **2015,** *9*, 831-839.

(35) Park, Y.-S.; Guo, S.; Makarov, N. S.; Klimov, V. I., Room Temperature Single-Photon Emission from Individual Perovskite Quantum Dots. *ACS Nano* **2015,** *9*, 10386-10393.

(36) Rainò, G.; Nedelcu, G.; Protesescu, L.; Bodnarchuk, M. I.; Kovalenko, M. V.; Mahrt, R. F.; Stöferle, T., Single Cesium Lead Halide Perovskite Nanocrystals at Low Temperature: Fast Single-Photon Emission, Reduced Blinking, and Exciton Fine Structure. *ACS Nano* **2016,** *10*, 2485-2490.

(37) Utzat, H.; Shulenberger, K. E.; Achorn, O. B.; Nasilowski, M.; Sinclair, T. S.; Bawendi, M. G., Probing Linewidths and Biexciton Quantum Yields of Single Cesium Lead Halide Nanocrystals in Solution. *Nano Letters* **2017,** *17*, 6838-6846.

(38) Yarita, N.; Tahara, H.; Saruyama, M.; Kawawaki, T.; Sato, R.; Teranishi, T.; Kanemitsu, Y., Impact of Postsynthetic Surface Modification on Photoluminescence Intermittency in Formamidinium Lead Bromide Perovskite Nanocrystals. *The Journal of Physical Chemistry Letters* **2017,** *8*, 6041-6047.

(39) Freppon, D. J.; Men, L.; Burkhow, S. J.; Petrich, J. W.; Vela, J.; Smith, E. A., Photophysical Properties of Wavelength-Tunable Methylammonium Lead Halide Perovskite Nanocrystals. *Journal of Materials Chemistry C* **2017,** *5*, 118-126.

(40) Zhang, A.; Dong, C.; Ren, J., Tuning Blinking Behavior of Highly Luminescent Cesium Lead Halide Nanocrystals through Varying Halide Composition. *The Journal of Physical Chemistry C* **2017,** *121*, 13314-13323.

(41) Gibson, N. A.; Koscher, B. A.; Alivisatos, A. P.; Leone, S. R., Excitation Intensity Dependence of Photoluminescence Blinking in $CsPbBr_3$ Perovskite Nanocrystals. *The Journal of Physical Chemistry C* **2018,** *122*, 12106-12113.

(42) Seth, S.; Ahmed, T.; Samanta, A., Photoluminescence Flickering and Blinking of Single $CsPbBr_3$ Perovskite Nanocrystals: Revealing Explicit Carrier Recombination Dynamics. *The Journal of Physical Chemistry Letters* **2018,** *9*, 7007-7014.

(43) Yuan, G.; Ritchie, C.; Ritter, M.; Murphy, S.; Gómez, D. E.; Mulvaney, P., The Degradation and Blinking of Single $CsPbI_3$ Perovskite Quantum Dots. *The Journal of Physical Chemistry C* **2018,** *122*, 13407-13415.

(44) Tian, Y.; Merdasa, A.; Peter, M.; Abdellah, M.; Zheng, K.; Ponseca, C. S.; Pullerits, T.; Yartsev, A.; Sundström, V.; Scheblykin, I. G., Giant Photoluminescence Blinking of Perovskite Nanocrystals Reveals Single-Trap Control of Luminescence. *Nano Letters* **2015,** *15*, 1603-1608.

(45) Ryan, D. P.; Goodwin, P. M.; Sheehan, C. J.; Whitcomb, K. J.; Gelfand, M. P.; Van Orden, A., Mapping Emission from Clusters of CdSe/ZnS Nanoparticles. *The Journal of Physical Chemistry C* **2018,** *122*, 4046-4053.

(46) Pennycook, S. J.; Jesson, D. E., High-Resolution Z-Contrast Imaging of Crystals. *Ultramicroscopy* **1991,** *37*, 14-38.

(47) Linaburg, M. R.; McClure, E. T.; Majher, J. D.; Woodward, P. M., $Cs_{1-x}Rb_xPbCl_3$ and $Cs_{1-x}Rb_xPbCl_3$ Solid Solutions: Understanding Octahedral Tilting in Lead Halide Perovskites. *Chemistry of Materials* **2017,** *29*, 3507-3514.

(48) Akkerman, Q. A.; Motti, S. G.; Srimath Kandada, A. R.; Mosconi, E.; D'Innocenzo, V.; Bertoni, G.; Marras, S.; Kamino, B. A.; Miranda, L.; De Angelis, F*., et al.*, Solution Synthesis Approach to Colloidal Cesium Lead Halide Perovskite Nanoplatelets with Monolayer-Level Thickness Control. *Journal of the American Chemical Society* **2016,** *138*, 1010-1016.

(49) Abdelmageed, G.; Jewell, L.; Hellier, K.; Seymour, L.; Luo, B.; Bridges, F.; Zhang, J. Z.; Carter, S., Mechanisms for Light Induced Degradation in $MAPbI_3$ Perovskite Thin Films and Solar Cells. *Applied Physics Letters* **2016,** *109*, 233905.

(50) Draguta, S.; Sharia, O.; Yoon, S. J.; Brennan, M. C.; Morozov, Y. V.; Manser, J. S.; Kamat, P. V.; Schneider, W. F.; Kuno, M., Rationalizing the Light-Induced Phase Separation of Mixed Halide Organic–Inorganic Perovskites. *Nature Communications* **2017,** *8*, 200-1-8.

(51) Song, Z.; Wang, C.; Phillips, A. B.; Grice, C. R.; Zhao, D.; Yu, Y.; Chen, C.; Li, C.; Yin, X.; Ellingson, R. J.*, et al.*, Probing the Origins of Photodegradation in Organic–Inorganic Metal Halide Perovskites with Time-Resolved Mass Spectrometry. *Sustainable Energy & Fuels* **2018,** *2*, 2460-2467.

(52) Liu, L.; Deng, L.; Huang, S.; Zhang, P.; Linnros, J.; Zhong, H.; Sychugov, I., Photodegradation of Organometal Hybrid Perovskite Nanocrystals: Clarifying the Role of Oxygen by Single-Dot Photoluminescence. *The Journal of Physical Chemistry Letters* **2019,** *10*, 864-869.

(53) Yang, J.-H.; Yin, W.-J.; Park, J.-S.; Wei, S.-H., Fast Self-Diffusion of Ions in $CH_3NH_3PbI_3$: The Interstiticaly Mechanism Versus Vacancy-Assisted Mechanism. *Journal of Materials Chemistry A* **2016,** *4*, 13105-13112.

(54) Ott, F. D.; Spiegel, L. L.; Norris, D. J.; Erwin, S. C., Microscopic Theory of Cation Exchange in CdSe Nanocrystals. *Physical Review Letters* **2014,** *113*, 156803.

(55) Senocrate, A.; Moudrakovski, I.; Kim, G. Y.; Yang, T.-Y.; Gregori, G.; Grätzel, M.; Maier, J., The Nature of Ion Conduction in Methylammonium Lead Iodide: A Multimethod Approach. *Angewandte Chemie International Edition* **2017,** *56*, 7755-7759.

(56) Nightingale, A. M.; Bannock, J. H.; Krishnadasan, S. H.; O'Mahony, F. T. F.; Haque, S. A.; Sloan, J.; Drury, C.; McIntyre, R.; deMello, J. C., Large-Scale Synthesis of Nanocrystals in a Multichannel Droplet Reactor. *Journal of Materials Chemistry A* **2013,** *1*, 4067-4076.

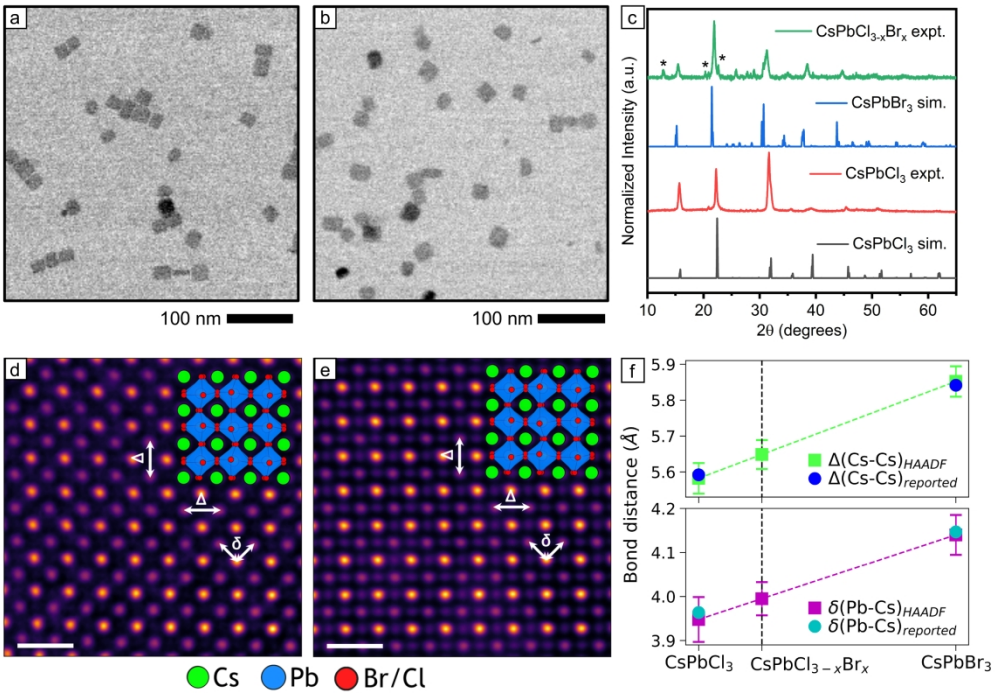

Figure 1

266x184mm (300 x 300 DPI)

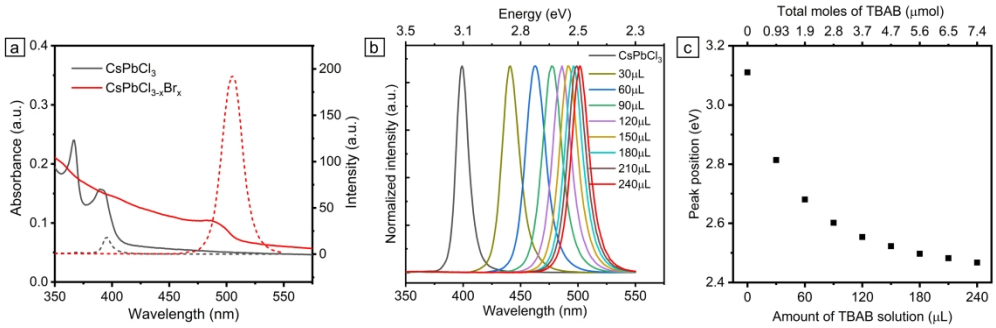

Figure 2

295x96mm (300 x 300 DPI)

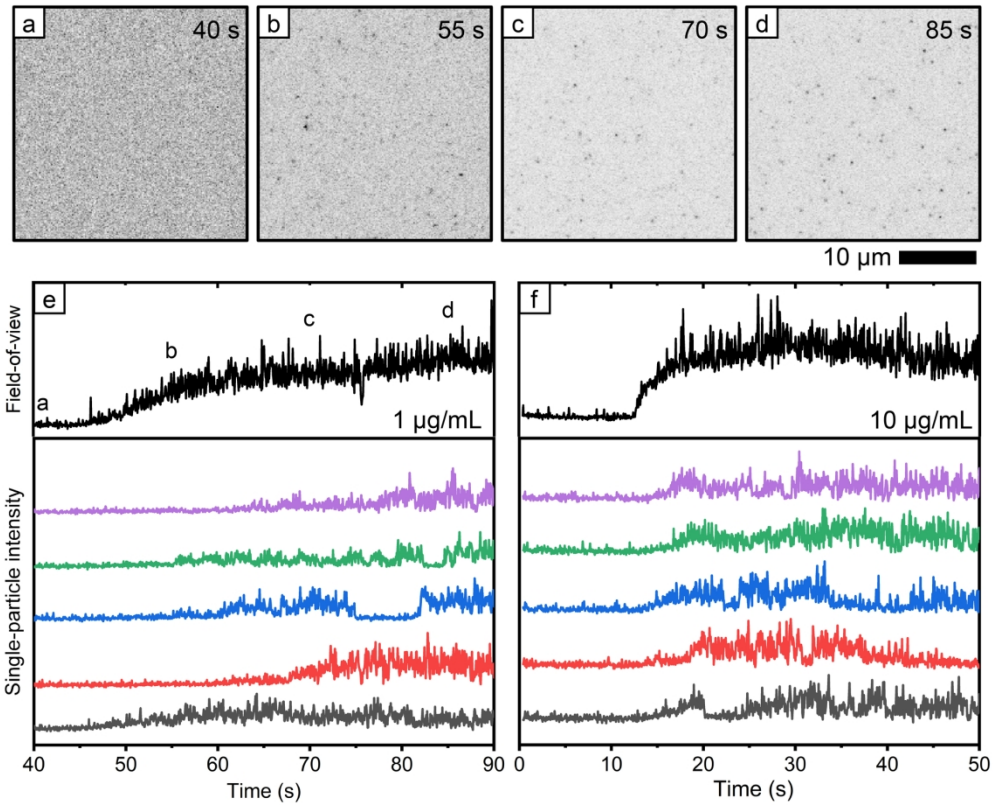

Figure 3

171x137mm (300 x 300 DPI)

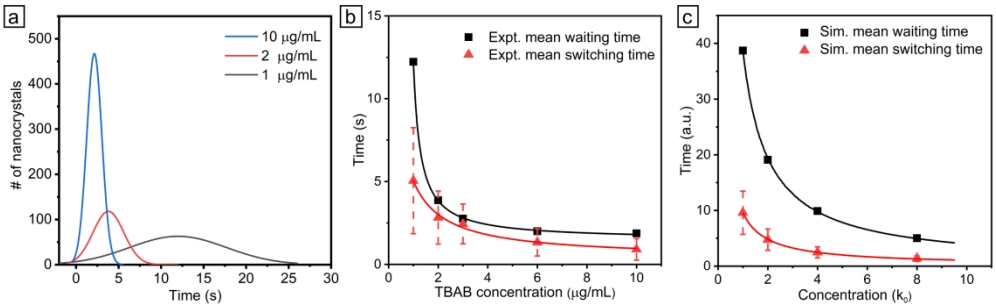

Figure 4

247x76mm (300 x 300 DPI)